Analysis of Effects of Rebounds and Aerodynamics for Trajectory of Table Tennis Ball

Junko Nonomura
Mechanical Science and Engineering,
Graduate School of Engineering,
Nagoya University,
Furo-cho, Chikusa-ku,
Nagoya, Japan

Akira Nakashima
Mechanical Science and Engineering,
Graduate School of Engineering,
Nagoya University,
Furo-cho, Chikusa-ku,
Nagoya, Japan

Yoshikazu Hayakawa
Mechanical Science and Engineering,
Graduate School of Engineering,
Nagoya University,
Furo-cho, Chikusa-ku,
Nagoya, Japan
and RIKEN-TRI Collaboration Center,
RIKEN, 2271-103, Anagahora,
Shimoshidami, Moriyama-ku,
Nagoya, Japan

***Abstract*—In this paper, we firstly analyze the effects of the rebounds and aerodynamics for trajectory of a table tennis ball. We firstly analyze the effect of the aerodynamics with a criterion of evaluation, where the half area of the table is considered as 9 divided areas. Furthermore, the drag and lift coefficients are identified by assuming that the rotational velocity is invalid during the ball flying. With the identified coefficients, the modeling errors of the table and racket are secondly verified by the criterion mentioned previously. Some conclusions are finally shown.**

***Index Terms*—Ball trajectory, Rebound Phenomenon, aerodynamics, Table tennis**

I. Introduction

A human detect a lot of information of external world with his eyes, i.e., the sense of vision. With the obtained information, he extract some useful specified information which is necessary for tasks, e.g., catching, throwing and hitting a ball, and so on. Therefore, it is very important and useful for a robot in uncertain environment to use vision sensors and have algorithms for objective tasks with its obtained vision information.

We aim to realize a robot to play table tennis with a human as a typical example of robots in uncertain environment since playing table tennis is a dexterous task for humans. For simplicity, consider the situation shown in Fig. 1, where a robot try to hit a flying ball. In this situation, the strategy of the robot can be decomposed as the following subtasks:

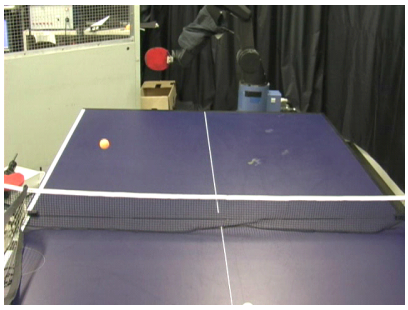

Fig. 1. A robot tries to hit a flying ball.

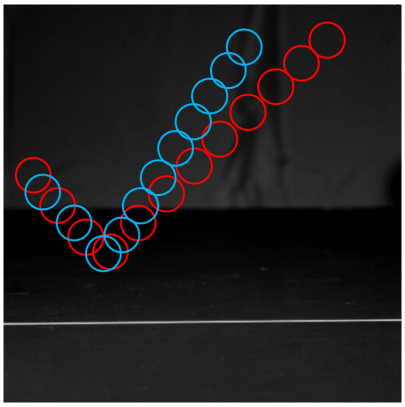

Fig. 2. Ball trajectories of the cases of the top or back spin.

1) To detect the states of the flying ball with vision sensors.
2) To predict the ball trajectory.
3) To determine the trajectory of the racket attached to the robot for the hitting to achieve desired ball trajectory.

The number 1) means the image processing algorithm to obtain the position, the translational velocity and the rotational velocity of the ball. This algorithm is needed to performed in real time for the next task of the prediction[2]. The number 2) means the prediction of the position and translational/rotational velocities of the ball for the next task of the determination. The number 3) means the determination of the trajectory of the position and orientation of the racket for the ball to follow desired trajectory. In the subtasks 2) and 3), the ball rebounds from the table and the racket rubber. Furthermore, the flying ball is affected by aerodynamic forces. It is therefore necessary to model the rebounds and the aerodynamics. Suppose in this paper that the translational and rotational velocities can be measured by an appropriate method[2]. Therefore, we concern on the analysis of effects which should be considered in the prediction of the ball

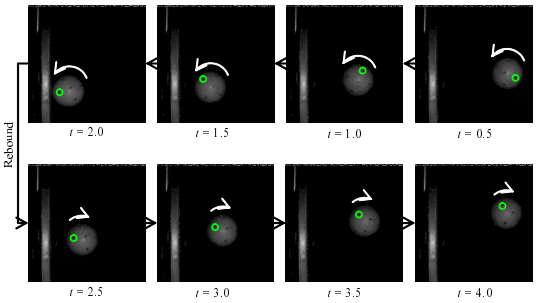

Fig. 3. Rebound of the ball from the racket rubber.

trajectory. In Fig. 2, the red and blue circles represent the cases of the top. The back spins respectively and the ball velocity just before the rebound is the same as the each other case. It is easily confirmed that the velocity normal to the table in the case of the back spin is greater than that in the case of the top spin. In addition, the rotational velocity after rebound also changes due to the friction. In order to predict the ball trajectory after the rebound from the table, it is necessary to consider the friction of the table[1]. Second, let us consider the rebound phenomenon between the ball and the racket rubber. Fig. 3 shows an example of the rebound of the ball from the racket rubber. The green circles represent the same point on the ball. It is confirmed that the rotational velocity about the axis normal to the images changes to the *inverse* direction after the rebound. This can not be expressed by considering only the friction and is the specific phenomenon in the case of the rubber. In order to achieve desired ball trajectory after the rebound from the racket, it is necessary to consider this phenomenon[1]. Finally, we should consider the effect of the aerodynamic forces. Fig. 4 shows the aerodynamic forces for a flying ball, i.e., *lift* and *drag*. The lift is proportional to the spinning of the ball. The drag disturbs the ball motion and is proportional to the translational velocity. The trajectory of the ball changes easily by these two effects since the weight of the ball is small and the rotation velocity is high, e.g., 3000[rpm]. In order to achieve desired ball trajectory after the rebound, it is necessary to consider these phenomena.

In this paper, we analyze the effects of the rebounds and aerodynamics for trajectory of a table tennis ball. We firstly analyze the effect of the aerodynamics with a criterion of evaluation, where the half area of the table is considered as 9 divided areas. Furthermore, the drag and lift coefficients are identified by assuming that the rotational velocity is invalid during the ball flying. With the identified coefficients, the modeling errors of the table and racket are secondly verified by the criterion mentioned previously. Some conclusions are finally shown.

II. Rebound Models of Table and Racket Rubber

A. Rebound Model of Table

Fig. 5 shows the rebound of the ball from the table, where ($\boldsymbol{v}_b$,$\boldsymbol{\omega}_b$) and ($\boldsymbol{v}'_b, \boldsymbol{\omega}'_b$)are the translational and rotational velocities of the ball just before and after the rebound. Σ_B is the reference frame with the z-axis normal to the table. Since there exists the friction between the ball and the table, the velocities $\boldsymbol{v}_b$ changes to $\boldsymbol{v}'_b$.

The model between table and the ball is given by (5) and (6)[1]. It is very important to consider the *type of the contact* during the impact, i.e., the sliding and rolling contact. This can be determined by using the tangent velocity given by

$$\boldsymbol{v}_{bT} := [v_{bx}\ v_{by}\ 0]^{\mathrm{T}} + \boldsymbol{\omega} \times \boldsymbol{r} = \begin{bmatrix} v_{bx} - r\omega_{by} \\ v_{by} + r\omega_{bx} \\ 0 \end{bmatrix}, \quad (1)$$

where $\boldsymbol{r} := [0\ 0\ -r]^{\mathrm{T}} \in \mathbb{R}^3$ is the contact point of the ball from its center and $r \in \mathbb{R}_+$ is the ball radius. For the modeling, we make the following assumptions:

Assumption 1: During the impact of the rebound, the type of the contact between the ball and table is a point contact. This means that any moment does not effect on the ball during the impact.

Assumption 2: The differences between the translational and angular momentums before and after the rebound equal the impulses at the rebound. Therefore, the impulse of the rotation is given by $\boldsymbol{r} \times \boldsymbol{P}$, where $\boldsymbol{P} \in \mathbb{R}^3$ is the impulse in the translational direction.

Assumption 3: The following simple bounce relationship in the z direction holds:

$$v'_{bz} = -e_t v_{bz} \quad (2)$$

Assumption 4: The impulse in the x and y directions $\boldsymbol{P}_{xy} := [P_x\ P_y\ 0]^{\mathrm{T}} \in \mathbb{R}^3$ is given by

$$\boldsymbol{P}_{xy} = -\lambda \frac{\boldsymbol{v}_{bT}}{\|\boldsymbol{v}_{bT}\|},\ 0 \le \lambda \le \mu |P_z|, \quad (3)$$

where μ is the dynamical coefficient of friction between the ball and table.

Assumption 5: The contact velocities $\boldsymbol{v}_b$ and $\boldsymbol{v}'_b$ just before and after the rebound are in the same direction. That is, the following relation holds:

$$\boldsymbol{v}'_{bT} = \nu \boldsymbol{v}_{bT},\ \nu \ge 0. \quad (4)$$

If $\nu \neq 0$, $\lambda = \mu |P_z|$.
From Assumptions, the following rebound model is derived[1].

$$\boldsymbol{v}'_b = \boldsymbol{A}_v \boldsymbol{v}_b + \boldsymbol{B}_v \boldsymbol{\omega}_b \quad (5)$$

$$\boldsymbol{\omega}'_b = \boldsymbol{A}_\omega \boldsymbol{v}_b + \boldsymbol{B}_\omega \boldsymbol{\omega}_b. \quad (6)$$

where

$$\boldsymbol{A}_v := \begin{bmatrix} 1-\alpha & 0 & 0 \\ 1 & 1-\alpha & 0 \\ 0 & 0 & -e_t \end{bmatrix}, \boldsymbol{B}_v := \begin{bmatrix} 0 & \alpha r & 0 \\ -\alpha r & 0 & 0 \\ 0 & 0 & 0 \end{bmatrix}$$

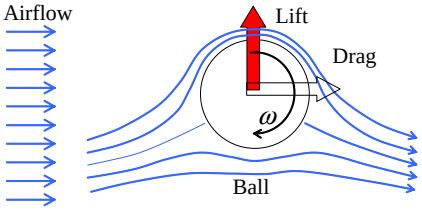

Fig. 4. Lift and Drag of aerodynamics.

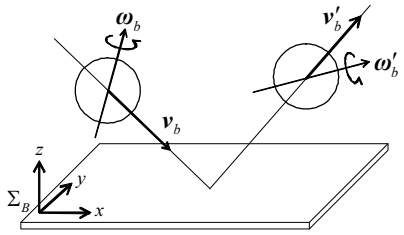

Fig. 5. Ball velocities just before and after the rebound

$$\boldsymbol{A}_\omega := \begin{bmatrix} 0 & -\frac{3\alpha}{2r} & 0 \\ \frac{3\alpha}{2r} & 0 & 0 \\ 0 & 0 & 0 \end{bmatrix}, \boldsymbol{B}_\omega := \begin{bmatrix} 1-\frac{3\alpha}{2} & 0 & 0 \\ 0 & 1-\frac{3\alpha}{2} & 0 \\ 0 & 0 & 1 \end{bmatrix}$$

$$\alpha = \begin{cases} \mu(1+e_t)\frac{|v_{bz}|}{\|\boldsymbol{v}_{bT}\|} & (\nu_s > 0) \\ \frac{2}{5} & (\nu_s \le 0) \end{cases}$$

$$\nu_s = 1 - \frac{2}{5}\mu(1+e_t)\frac{|v_{bz}|}{\|\boldsymbol{v}_{bT}\|}.$$

$\nu_s > 0$ means the case of the sliding contact and $\nu_s \le 0$ means the case of the rolling contance.

B. Rebound Model of Racket Rubber

Fig. 6 shows the rebound of the ball from the racket rubber, where the meanings of the variables are the same as in SubsectionII-A with respect to the racket frame Σ_R attached to the racket as the z-axis normal to the surface. In order to express the effect of the elasticity parallel to the surface,

For the model, we make the following assumptions:

Assumption 6: The rebound in the z direction does not cause any effect in the x and y directions.

Assumption 7: The impulse in the x and y directions $\boldsymbol{P}_{xy} \in \mathbb{R}^3$ is related to the tangent velocity $\boldsymbol{v}_{bT}$ by

$$\boldsymbol{P}_{xy} = -k_p \boldsymbol{v}_{bT}. \tag{7}$$

From Assumption 1-3, 6 and 7, the rebound model of the racket is derived as the same form as (5) and (6).

The coefficient matrices are as follows:

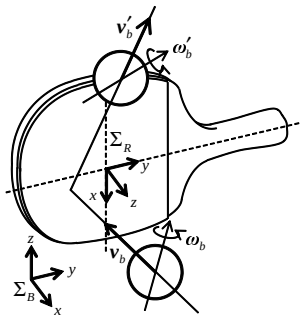

(a) Rebound between the ball and the rubber

Fig. 6. Racket Coordinate.

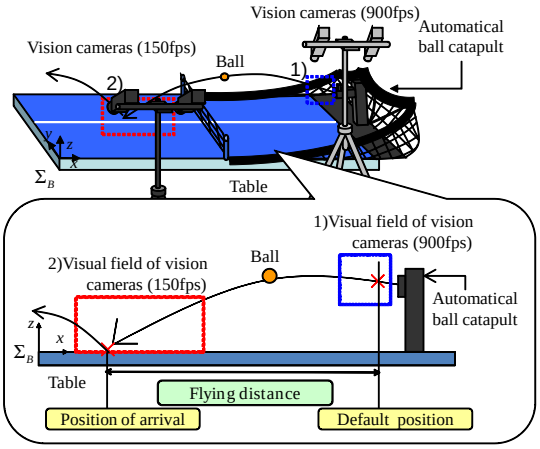

Fig. 7. Experimental system and flying distance.

$$\boldsymbol{A}_v := \begin{bmatrix} 1-K_v & 0 & 0 \\ 0 & 1-K_v & 0 \\ -e_r & 0 & 0 \end{bmatrix}, \boldsymbol{B}_v := K_v \begin{bmatrix} 0 & r & 0 \\ -r & 0 & 0 \\ 0 & 0 & 0 \end{bmatrix}$$

$$\boldsymbol{A}_\omega := K_\omega \begin{bmatrix} 0 & -r & 0 \\ r & 0 & 0 \\ 0 & 0 & 0 \end{bmatrix}, \boldsymbol{B}_\omega := \begin{bmatrix} 1-K_\omega r^2 & 0 & 0 \\ 0 & 1-K_\omega r^2 & 0 \\ 0 & 0 & 1 \end{bmatrix}$$

$$K_v := \frac{k_p}{m},\ k_\omega := \frac{k_p}{I}$$

where e_r is the coefficient of restitution of the rubber.

III. Ball Motion with Aerodynamics

The ball motion is expressed by the free-fall equation if there is no aerodynamics. However in the real world, the flying ball is affected by the aerodynamics.

Fig. 7 shows the experimental system to detect the flying distance. The Σ_B is set the edge of the table. Balls are shot out from the automatic ball catapult and detected by 2 pairs of vision sensors. The sampling frequency of the right cameras is 900[fps]. These cameras are called high speed cameras. The initial position and translational/rotational velocities are detected by the high speed cameras. The sampling frequency of the right cameras is 150[fps]. These cameras are called middle speed cameras. The position of arrival is detected by these cameras. The blue square is the visual field of the

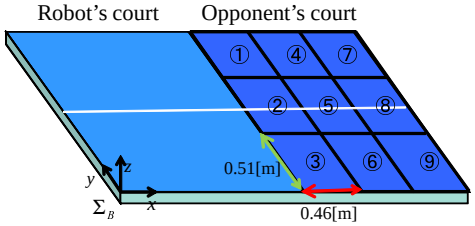

Fig. 8. Criterion of evaluation

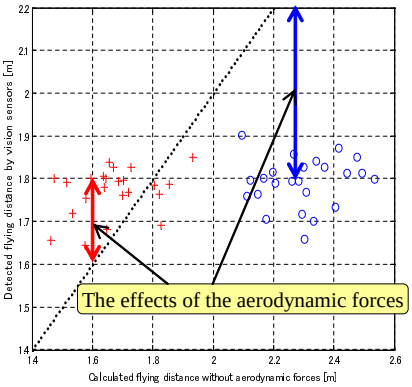

Fig. 9. The flying distance between the measured value and the calculated value without aerodynamic forces.

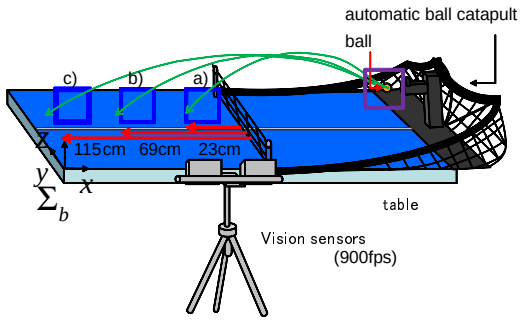

Fig. 10. Experiment system to confirm rotational velocity

high speed cameras and the red square shows that of the middle speed cameras. The flying distance is measured by this experimental system. For comparison, the flying distance in the case of the free ball motion is calculated using the measured initial position and velocity.

We use each 24 case of top spin ball and back spin ball. The initial translational velocity of the top/back spins are -6.2/-6.5[m/s] and the initial rotational velocity of the top/back spins are about -3400/3400[rpm] around the y axis of Σ_B. Fig. 8 shows the table area divided into 9 areas. The size of one area is $0.46 \times 0.51[\mathrm{m}^2]$. The influence of the aerodynamic forces are evaluated by the 9 divided areas since players may devise their strategies by choosing the one of these areas.

Fig. 9 shows the relation between the flying distances of the ball with and without aerodynamics. The horizontal/vertical axes are the calculated/measured flying distances. The dotted line means that the calculated values equal to the measured values. The circles and crosses represents the cases of the top and back. The differences between the dotted line and circles/crosses show the influence of the aerodynamic forces. The blue/red arrows show the influences in the case of top/back spin. The difference of the influence in the case of back spin is smaller than the case of top spin. However it is about 0.2[m] which is close to the half size of the sides of the divided areas.

Therefore, in order to hit into the desired area, it is necessary to consider the aerodynamic forces.

IV. Identification of Aerodynamics

As the model including Aerodynamics, (8) is introduced [3].

$$m\ddot{\boldsymbol{p}} = m\boldsymbol{g} - \frac{1}{2}C_D\rho A\|\dot{\boldsymbol{p}}\|\dot{\boldsymbol{p}} + \frac{4}{3}C_M\pi\rho r^3\boldsymbol{\omega}\times\dot{\boldsymbol{p}} \qquad (8)$$

where m: mass, $\boldsymbol{g}$: acceleration of gravity, ρ: air density, A: projected area, r: radius, C_D: drag coefficient, C_M: lift coefficient, $\boldsymbol{p}$: position of the ball, $\boldsymbol{\omega}$: rotational velocity.

The values are given by m=2.7×10^{-3}[kg], $\boldsymbol{g}$=$[0,0,-9.8]^T[\mathrm{m/s}^2]$, ρ=1.184 $[\mathrm{kg/m}^3](25^\circ\mathrm{C})$, A=$12.5\times10^{-4}[\mathrm{m}^2]$ and r=$20.0\times10^{-3}[\mathrm{m}]$.

In order to identify C_D and C_M, we assume that $\boldsymbol{\omega}$ is constant value. Fig. 10 shows the experimental system to confirm the assumption. Blue frames a), b) and c) are the visual fields of the high speed cameras. The frame a) is placed 23[cm] away from the center line and the frame b) and c) are away from 69[cm] and 115[cm], respectively. Balls are shot out from the automatic ball catapult parallel.

From Fig. 11 through Fig. 13 show the rotational velocity. The horizontal axis is the speed scale markings of the automatic ball catapult and the vertical axis is the rotational velocity detected by the vision sensors. The closed circles are the average of rotational velocity just after the time when the ball is shot by the automatic ball catapult. The black dotted line represents the standard variation of the rotational velocity. The blue line is the linearization of the closed circles. The pink cross shows the average of rotational velocity in the case of a) - c). The pink dotted line represents the standard variation of the rotational velocity in the each case $\pm3\sigma$.

All the pink crosses are contained in the area between the black dotted lines in the case of a) and b). Then, the rotational velocity can be assumed not to during the ball flying.

The coefficients of C_D and C_M are identified by minimizing the following cost function:

$$V(C;\boldsymbol{p}_i) := \frac{1}{2}\|\boldsymbol{p}_i(t) - \boldsymbol{p}(t;C)\| \qquad (9)$$

where $\boldsymbol{p}_i(t) \in \mathbb{R}^3$ is the measured ball trajectory (i=1,$\cdots$,N) and $\boldsymbol{p}(t;C) \in \mathbb{R}^3$, C:=$[C_D\ C_M] \in \mathbb{R}^2_+$ is obtained by solving (8) numerically with the initial values of $\boldsymbol{p}$ and $\dot{\boldsymbol{p}}$ which are given by $\boldsymbol{p}_i(0)$ and $\dot{\boldsymbol{p}}_i(0) \approx \frac{\boldsymbol{p}_i(\Delta t)-\boldsymbol{p}_i(0)}{\Delta t}, \Delta t = \frac{1}{150}$[s]. The minimization is dealt with for each data of $\boldsymbol{P}_i$(N=50). The identified C_D and C_M are 0.54$\pm$0.074 and 0.069$\pm$0.029. The result is verified by another data not to be used in the identification. An example is shown in Fig. 14 and Fig. 15. In Fig. 14 and Fig. 15, the blue, red and green lines represent the measured ball trajectory and the numerically simulated ones with and without the aerodynamics. It is confirmed that the red lines almost coincide with the blue lines.

V. Verification of Ball Trajectory

In older to use the model of the racket, we have to consider the arrival position of the ball which is hit by the racket. Fig. 16 shows the experimental system for the verification of

the racket rebound model, the ball is shot by the automatic ball catapult and the translational/rotational velocities just before and after the rebound from the racket are measured by the high speed cameras. The predicted positions of arrival are calculated using the aerodynamics (8) with the identified C_D and C_M and the translational/rotational velocities just after the rebound obtained from the rebound model. We verify the modeling error of the rebound from the racket based on the distance between the calculated and measured positions of arrival with the criterion the 9 divided areas. Fig. 17, Fig. 18 and Fig. 19 show the trajectory and the position of arrival. The blue line and dot represents initial translational/rotational velocity are given by the high speed cameras. The red line and dot represents initial translational/rotational velocity are given by the racket model. In the case of the top spin, the average error is 0.09[m] and the standard deviation is 0.03[m]. In the case of the back spin, the average error is 0.04[m] and the standard deviation is 0.04[m]. Because it is confirmed that the positions of arrival with all of the errors are included in one area, the model of the racket can be used for the prediction of the ball.

VI. Conclusion

In this paper, we analyzed the effects of the rebounds and aerodynamics for trajectory of a table tennis ball. We firstly analyzed the effect of the aerodynamics with a criterion of evaluation, where the half area of the table is considered as 9 divided areas. Furthermore, the drag and lift coefficients were identified by assuming that the rotational velocity is invalid during the ball flying. With the identified coefficients, the modeling errors of the table and racket secondly were verified by the criterion mentioned previously. Some conclusions are finally shown.

As future work ,it is necessary to consider the trajectory of the racket for a robot to hit the ball to a desired position of arrival.

References

[1] A. Nakashima, Y. Ogawa, Y. Kobayashi and Y. Hayakawa, "Modeling of Rebound Phenomenon of a Rigid Ball with Friction and Elastic Effects", Proceeding of ACC2010, Baltimore, Maryland, USA ,2010 (To appear)

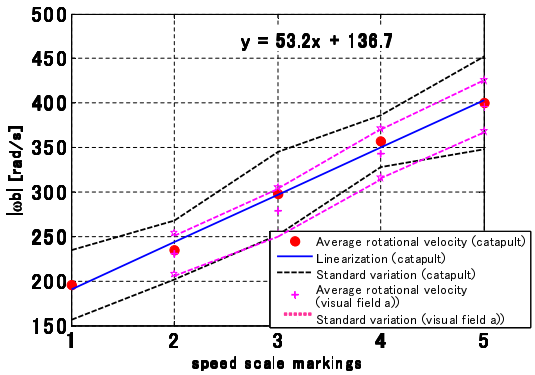

Fig. 11. Rotational velocity around the ball catapult and the frame a)

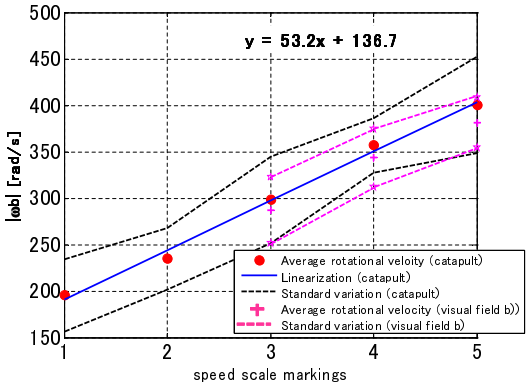

Fig. 12. Rotational velocity around the ball catapult and the frame b)

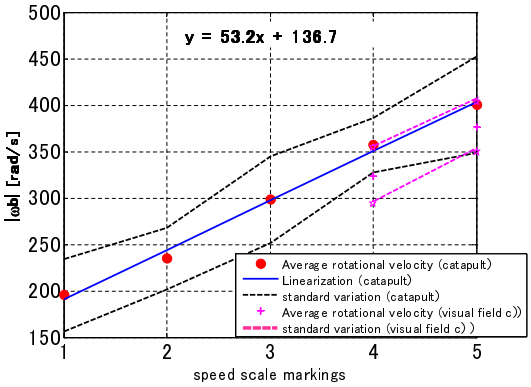

Fig. 13. Rotational velocity around the ball catapult and the frame c)

[2] A. Nakashima, Y. Tsuda, Y. Kobayashi and Y. Hayakawa, "A Real-Time Measuring Method of Translational/Rotational Velocities of a Flying Ball", Proc of IFAC Symp. Mech. Sys., Cambridge, Massachusetts, USA 2010(To be accepted)

[3] Naoki OKADA, Tomohiro YABUUCHI, Takuya FUNATOMI, Koh KAKUSHO and Michihiko MINOH, "Estimating Unobserved Motion of a Ball by Acquiring Its Physical Model from Image Sequences", IEICE, D vol.J91-D No.12, pp.2950-2960, 2008 (In Japanese)

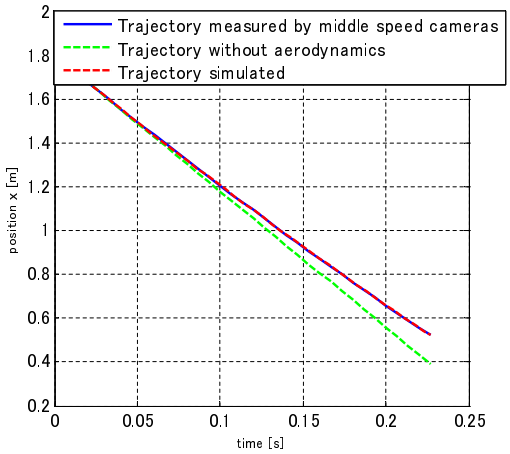

Fig. 14. Model identification and Trajectory in the direction of x axis

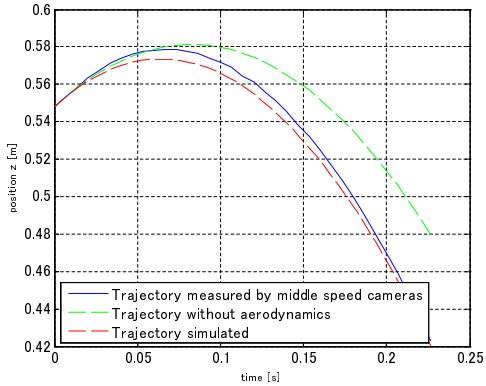

Fig. 15. Model identification and Trajectory in the direction of z axis

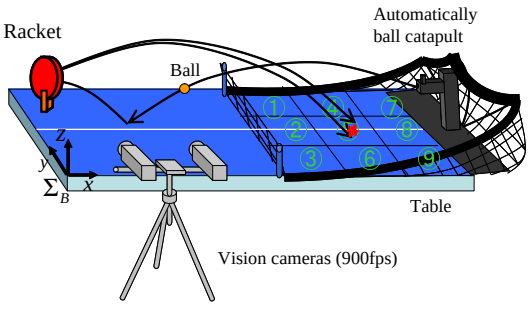

Fig. 16. Experimental system to verify the racket model

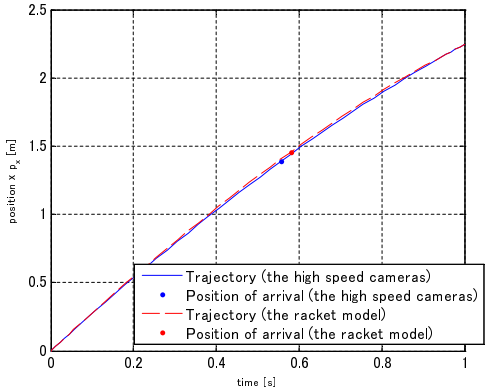

Fig. 17. Trajectory and arrival position in the direction of x axis

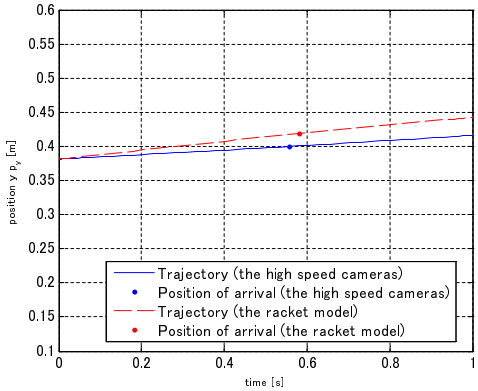

Fig. 18. Trajectory and arrival position in the direction of y axis

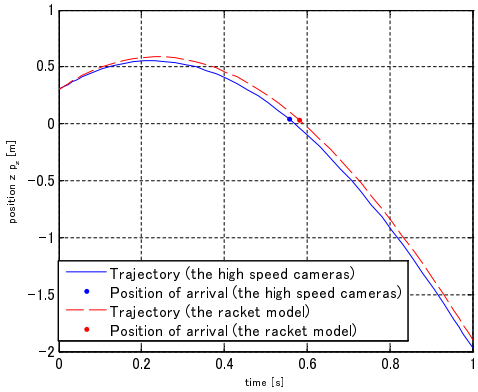

Fig. 19. Trajectory and arrival position in the direction of z axis